Mineralogical Magazine, August 2017, Vol. 81(4), pp. 841–855

Wiklundite, ideally $Pb_2^{[4]}(Mn^{2+},Zn)_3(Fe^{3+},Mn^{2+})_2(Mn^{2+},Mg)_{19}(As^{3+}O_3)_2[(Si,As^{5+})O_4]_6(OH)_{18}Cl_6$, a new mineral from Långban, Filipstad, Värmland, Sweden: Description and crystal structure

MARK A. COOPER[1], FRANK C. HAWTHORNE[1,*], JÖRGEN LANGHOF[2], ULF HÅLENIUS[2] AND DAN HOLTSTAM[2,3]

[1] Department of Geological Sciences, University of Manitoba, Winnipeg, Manitoba R3T 2N2, Canada
[2] Department of Geosciences, Swedish Museum of Natural History, Box 50007, SE-10405 Stockholm, Sweden
[3] Swedish Research Council, Box 1035, 101 38 Stockholm, Sweden

[*Received 21 April 2016; Accepted 10 July 2016; Associate Editor: Ed Grew*]

ABSTRACT

Wiklundite, ideally $Pb_2^{[4]}(Mn^{2+},Zn)_3(Fe^{3+},Mn^{2+})_2(Mn^{2+},Mg)_{19}(As^{3+}O_3)_2[(Si,As^{5+})O_4]_6(OH)_{18}Cl_6$, is a new arseno-silicate mineral from Långban, Filipstad, Värmland, Sweden. Both the mineral and the name have been approved by the Commission on New Minerals, Nomenclature and Classification of the International Mineralogical Association (IMA 2015-057). Wiklundite and a disordered wiklundite-like mineral form radiating, sheaf-like aggregates (up to 1 mm long) of thin brownish-red and slightly bent lath-shaped crystals. It occurs in a dolomite-rich skarn in association with tephroite, mimetite, turneaurite, johnbaumite, jacobsite, barite, native lead, filipstadite and parwelite. Wiklundite is reddish brown to dark brown, and the streak is pale yellowish brown. The lustre is resinous to sub-metallic, almost somewhat bronzy, and wiklundite does not fluoresce under ultraviolet light. The calculated density is 4.072 g cm^{-3}. Wiklundite is brittle with an irregular fracture, and has perfect cleavage on {001}; no parting or twinning was observed. Wiklundite is uniaxial (–), orange red and non-pleochroic in transmitted light, but shows incomplete extinction and distorted interference figures, preventing complete determination of optical properties. Electron-microprobe analysis (H_2O calculated from the structure) of wiklundite gave SiO_2 11.17, Al_2O_3 0.06, Fe_2O_3 4.46, As_2O_5 0.75, As_2O_3 6.81, MnO 47.89, ZnO 0.78, CaO 0.09, PbO 14.48, Cl 6.65, H_2O 5.18, O=Cl_2 –1.50, total 97.11 wt.%, As valences and H_2O content taken from the crystal-structure refinement, and $Fe^{3+}/(Fe^{2+} + Fe^{3+})$ determined by Mössbauer spectroscopy. Wiklundite is hexagonal-rhombohedral, space group $R\bar{3}c$, $a = 8.257(2)$, $c = 126.59(4)$ Å, $V = 7474(6)$ Å^3, $Z = 6$. The crystal structure of wiklundite was solved by direct methods and refined to a final R_1 index of 3.2%. The structure consists of a stacking of five layers of polyhedra: three layers consist of trimers of edge-sharing Mn^{2+}-dominant octahedra linked by (SiO_4) tetrahedra, ($Fe^{3+}(OH)_6$) dominant octahedra and (AsO_3) triangular pyramids; one layer of corner-sharing (SiO_4) and ($Mn^{2+}O_4$) tetrahedra; and one layer of ($Mn^{2+}Cl_6$) octahedra and ($Pb^{2+}(OH)_3Cl_6$) polyhedra. The mineral is named after Markus Wiklund (*b*. 1969) and Stefan Wiklund (*b*. 1972), the well-known Swedish mineral collectors who jointly found the specimen containing the mineral.

KEYWORDS: Wiklundite, new mineral, arseno-silicate, crystal-structure refinement, electron-microprobe analysis, Långban, Sweden.

Introduction

SEVERAL related arseno-silicate minerals with structures based on complex heteropolyhedron stacking sequences are known: carlfrancisite

*E-mail: frank_hawthorne@umanitoba.ca
https://doi.org/10.1180/minmag.2016.080.136

(Hawthorne *et al.*, 2013); dixenite (Araki and Moore, 1981); kraisslite (Moore and Ito, 1978; Cooper and Hawthorne, 2012); mcgovernite (Palache and Bauer, 1927; Wuensch, 1960; Cooper and Hawthorne, 2001); turtmannite (Brugger *et al.*, 2001). Here we report on a new Pb–Mn–Fe–Cl arseno-silicate mineral from Långban, wiklundite, named after Markus Wiklund (b.1969) and Stefan Wiklund (b. 1972), the brothers who jointly found the specimen containing the mineral. They are well-known Swedish mineral collectors with a long and profound interest in the mineralogy of Långban. Through their active membership in the Långban Society, they are dedicated non-professional contributors to the mineralogy of the Långban-type deposits. Both the mineral and the name have been approved by the Commission on New Minerals, Nomenclature and Classification of the International Mineralogical Association (IMA 2015-057). The holotype specimen of wiklundite has been deposited in the collections of the Department of Geosciences, Swedish Museum of Natural History, Box 50007, SE-10405 Stockholm, Sweden, under collection number NRM#20040085.

Occurrence

The Långban Fe–Mn–(Ba–As–Pb–Sb) deposit, Filipstad district, Värmland, Sweden (59.85°N, 14.27°E), was discovered nearly half a millennium ago. It was mined, mainly for iron ore (hematite-magnetite), manganese ore (braunite-hausmannite), and dolomite rock, continuously for at least 250 years until 1972. Generally, the marble-hosted Långban-type deposits in the Bergslagen ore province were deposited originally from hydrothermal solutions as syngenetic chemical sediments in a submarine, high-f_{O_2}, active volcanic environment at c. 1.9 Ga (Boström *et al.*, 1979; Holtstam and Mansfeld, 2001). At Långban, deformed ore bodies, recrystallized skarn assemblages and several generations of cavity and late-stage fissure minerals bear witness to a subsequent complex geological evolution of the deposit during variable temperature-pressure regimes (Magnusson, 1930; Holtstam and Langhof, 1999). The mines display an intriguing mineral richness, with some 280 species reported, and 71 type minerals described so far, including structurally related dixenite (Flink, 1920) and arakiite (Roberts *et al.*, 2000).

Wiklundite was collected from dump material at the former extraction plant in the western part of the vast dump area at Långban during field collecting in May 2000. So far, only one specimen is known to have been found and its original position within the Långban ore bodies is unknown. The original sample, ~10 cm, was broken into several pieces and the matrix of the wiklundite-bearing type specimen (45 mm × 35 mm) consists mainly of dolomite and manganiferous calcite. Hausmannite and jacobsite occur as impregnations and the specimen has a poorly banded appearance. This type of association is often referred to as 'dirty dolomite' by advanced Långban collectors. The largest accumulation of wiklundite grains occurs, scattered almost like an impregnation, in a zone of semi-opaque grey-white manganiferous calcite. Here, the grain used for single-crystal analysis was collected. On the basis of energy dispersive spectroscopy (EDS) analyses made on a polished thin-section, the following associated minerals were encountered: tephroite, mimetite, turneaurite, johnbaumite, jacobsite, barite and native lead. In addition, some of the associated mimetite grains contain small inclusions of filipstadite and rare grains (<0.1 mm) of parwelite. A fissure filling, cutting the wiklundite-bearing matrix, contains hematite, caryopilite, minor calcite and a black manganese-oxyhydroxide mineral. Wiklundite most probably crystallized during skarn-forming processes shortly after peak metamorphism at temperatures above 600°C and moderate pressures

FIG. 1. Aggregates of radiating lath-shaped wiklundite crystals, showing typical very dark reddish brown colour and lustre. The fine-grained grey white matrix consists of manganiferous calcite. Field of view is 1.5 mm. Photo: Torbjörn Lorin.

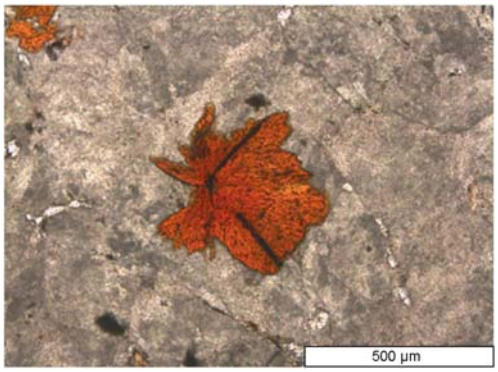

FIG. 2. An aggregate of lath-shaped wiklundite crystals in a fine-grained matrix of manganiferous calcite in polarized light.

of <3.5 kbar (Grew *et al.*, 1994; Christy and Gatedal, 2005).

Physical properties

Wiklundite and a wiklundite-like mineral form radiating, sheaf-like aggregates up to 1 mm, of thin brownish-red and slightly bent lath-shaped crystals (Figs 1 and 2), with the wiklundite-like mineral constituting the inner zone of each aggregate. Wiklundite is reddish brown to dark brown, and the lighter colour is typically seen in thinner fragments that show internal reflections; the streak is pale yellowish-brown. The lustre on the faces of the laths is resinous to sub-metallic, almost somewhat bronzy, whereas the edges of the laths are resinous. Wiklundite does not fluoresce under ultraviolet light. Mohs hardness and density could not be measured because of the size and shape of the crystals; the calculated density is 4.072 g cm^{-3}. Wiklundite is brittle with an irregular fracture, and has perfect cleavage on {001}; no parting or twinning was observed. The *c*:*a* ratio calculated from the single-crystal unit-cell parameters is 1 : 15.33. The small grain size and occurrence of wiklundite in sheaf-like aggregates, which causes incomplete extinction and distorted interference figures, made the complete determination of the optical properties not possible. Wiklundite is orange red and non-pleochroic in transmitted light, uniaxial (–) and $\langle n \rangle_{calc.} = 1.85$.

Infrared spectroscopy

An unpolarized single-crystal FTIR spectrum (Fig. 3) was recorded at the Swedish Museum of Natural History with a Bruker Vertex 70 spectrometer attached to a Bruker Hyperion2000 IR-microscope, using ATR-techniques on a 10 µm × 10 µm area of the crystal used for electron

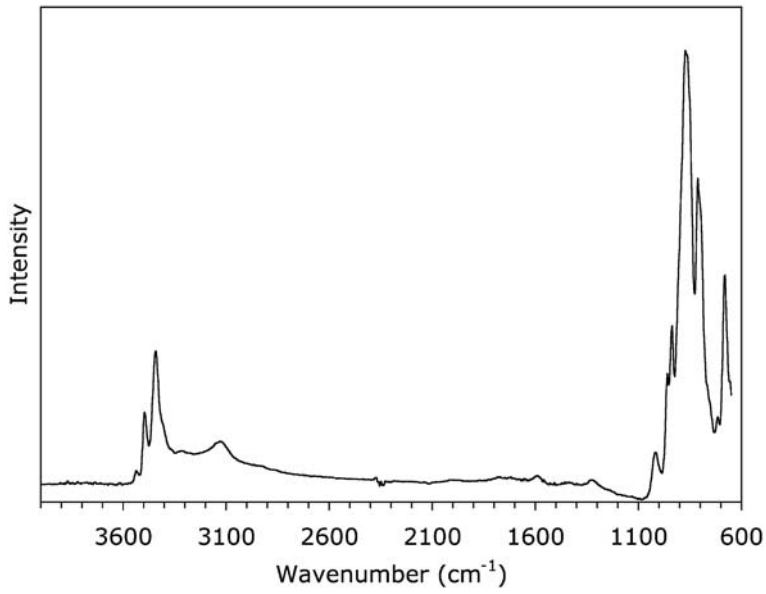

FIG. 3. Unpolarized, room-temperature Fourier transform infrared attenuated total reflection spectrum of wiklundite.

microprobe analysis (EMPA). The spectrum shows a set of absorption bands in the region 3100–3600 cm^{-1} (3128, 3316, 3404, 3441, 3496 and 3536 cm^{-1}) that may be ascribed to OH-stretching modes; there are only three crystallographically distinct (OH) groups, but the *M* sites adjacent to the groups contain more than one type of cation, and hence absorptions from different short-range arrangements of cations around each (OH) group give rise to different absorptions, cf. the situation in *C*2/*m* amphiboles in which a single (OH) group can give rise to six or more distinct absorption bands (Hawthorne and Della Ventura, 2007). There are intense bands related to AsO_4 modes, and subordinate SiO_4 and AsO_3 modes, in the 600–1000 cm^{-1} range (681, 712, 795, 813, 848, 861, 875, 938, 959 and 1020 cm^{-1}). Weak bands observed between 1300 and 2100 cm^{-1} are ascribed to overtones of these fundamental modes.

Mössbauer spectroscopy

A room-temperature ^{57}Fe Mössbauer spectrum was recorded on a very small quantity (≪1 mg) of powdered wiklundite using a WISSEL MA260S Mössbauer instrument operating in constant-acceleration mode (located at the Swedish Museum of Natural History). The spectrum was acquired by positioning an absorber consisting of mineral powder mixed with thermoplastic polymer close to a ^{57}Co point source in a rhodium matrix with a nominal activity of 10 mCi. The spectrum was calibrated against α–Fe and folded before fitting using the *MDA* software of Jernberg and Sundqvist (1983). The recorded spectrum shows one symmetrical absorption-doublet that is characterized by small peak-widths of 0.33 mm/s (Fig. 4) and a centroid shift (0.356 mm/s) typical for octahedrally coordinated Fe^{3+} (Coey, 1984). The quadrupole splitting of the doublet (0.264 mm/s) is small, which indicates that Fe^{3+} is coordinated by a regular octahedron of anions, resulting in an almost spherical electron distribution. The spectrum shows no indication of additional sites containing Fe^{3+} or the presence of Fe^{2+}.

Composition

Chemical analyses (8) of wiklundite were undertaken using a Cameca SX100 electron microprobe at the University of Manitoba: wavelength dispersive spectroscopy mode, 15 kV, 10 nA and 5 μm beam diameter. The following standards were used: PbTe (Pb), spessartine (Mn), gahnite (Zn), forsterite

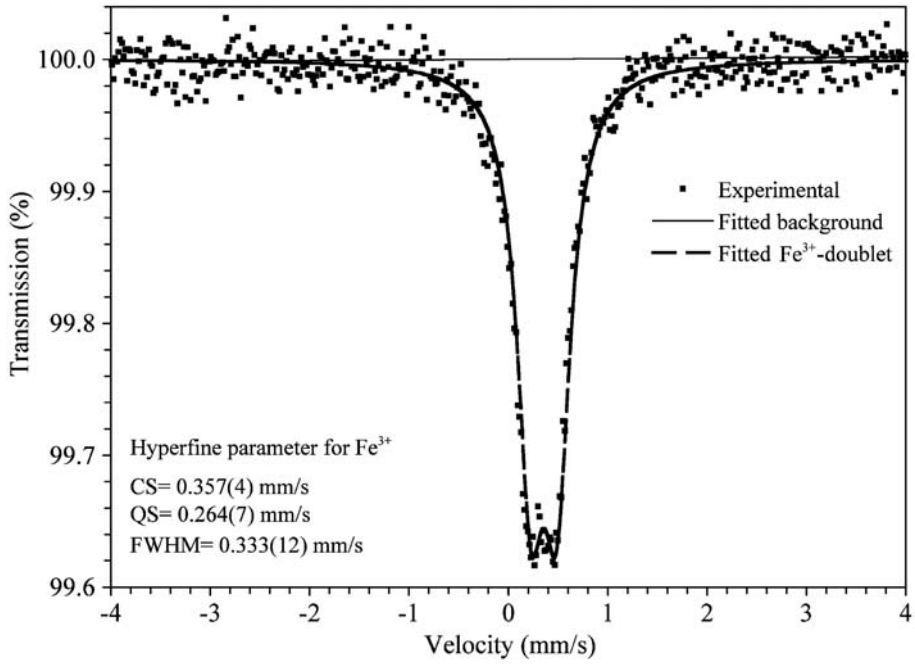

FIG. 4. Room temperature ^{57}Fe Mössbauer spectrum of wiklundite.

(Mg), diopside (Ca), fayalite (Fe, Si), andalusite (Al), cobaltite (As) and tugtupite (Cl). The elements Na, P, S, K, Ti, V, Cr, Cu, Sr, Sb, Ba and Bi were sought by EDS, but not detected. There was insufficient material for CHN (Carbon Hydrogen Nitrogen) analysis, so H_2O was calculated on the basis of 24 [(OH) + Cl] pfu (per formula unit) with $As^{3+}/(As^{3+} + As^{5+})$ taken from the crystal-structure solution and refinement. Data reduction was done using the *PAP* procedure of Pouchou and Pichoir (1985). The analytical results are given in Table 1. The analytical total is somewhat low; this is probably due to the fact that wiklundite polishes very poorly and the surface is rather irregular. The empirical formula (based on 54 anions $[O_{30}(OH + Cl)_{24}]$ apfu with all Fe as Fe^{3+} as indicated by Mössbauer spectroscopy (Fig. 4) is as follows: $Pb_{2.04}(Mn^{2+}_{2.70}Zn_{0.30})_{\Sigma 3.00}(Fe^{3+}_{1.76}Al_{0.04}Mn^{2+}_{0.20})_{\Sigma 2.00}(Mn^{2+}_{18.33}Mg_{0.23}Ca_{0.05})_{\Sigma 18.61}As^{3+}_{2.16}(Si_{5.85}As^{5+}_{0.21})_{\Sigma 6.06}O_{30}(OH)_{18.10}Cl_{5.90}$.

The simplified formula is: $Pb_2^{[4]}(Mn^{2+},Zn)_3(Fe^{3+},Mn^{2+})_2(Mn^{2+},Mg)_{19}(As^{3+}O_3)_2[(Si,As^{5+})O_4]_6(OH)_{18}Cl_6$.

Powder X-ray diffraction

The nature of the sample did not provide sufficient amounts of wiklundite to allow the collection of powder-diffraction data, as it is intimately intergrown at a very fine scale with at least one other phase of similar composition. Thus we collapsed the single-crystal X-ray intensity data to produce an experimental diffraction pattern that

TABLE 1. Chemical composition (wt.%) of wiklundite.

Constituent	Mean	Range	SD
PbO	14.48	13.10–15.10	0.78
MnO	47.89	47.34–48.37	0.34
ZnO	0.78	0.60–0.90	0.08
MgO	0.29	0.15–0.62	0.19
CaO	0.09	0.07–0.13	0.02
Fe_2O_3	4.46	4.23–4.78	0.17
Al_2O_3	0.06	0.03–0.08	0.01
$As_2O_3^{tot}$	7.46	7.08–8.03	0.28
As_2O_3	6.81[1]	—	—
As_2O_5	0.75[1]	—	—
SiO_2	11.17	11.02–11.31	0.09
Cl	6.65	5.96–7.04	0.34
H_2O[2]	5.18	—	—
O = Cl	–1.50	—	—
Total	97.11	—	—

[1]Calculated from the crystal-structure refinement;
[2]using (OH + Cl) = 24 apfu from the crystal-structure refinement.

TABLE 2. Simulated powder X-ray diffraction data (Mo$K\alpha$ = 0.71073 Å) for wiklundite derived from single-crystal X-ray intensity data.

I (%)	*d* (Å)	*h k l*	I (%)	*d* (Å)	*h k l*
2	21.084*	0 0 6	8	2.257	$\bar{3}$ 3 18
34	7.104	0 1 2	9	2.232	$\bar{1}$ 3 32
27	6.978	$\bar{1}$ 1 4	15	2.187	$\bar{2}$ 3 34
2	6.517	0 1 8	19	2.172	$\bar{3}$ 3 24
7	6.226	$\bar{1}$ 1 10	"	2.172	0 3 24
4	5.609	0 1 14	2	2.109	0 0 60
20	5.301	$\bar{1}$ 1 16	8	2.087	$\bar{1}$ 1 58
40	**4.740**	**0 1 20**	12	2.064	$\bar{2}$ 4 0
10	4.483	$\bar{1}$ 1 22	14	2.055	$\bar{2}$ 4 6
7	4.215	0 0 30	8	2.033	$\bar{1}$ 3 41
83	**4.128**	**$\bar{1}$ 2 0**	9	2.026	$\bar{2}$ 4 12
58	**4.052**	**$\bar{1}$ 2 6**	3	2.004	$\bar{2}$ 4 15
10	3.962	$\bar{1}$ 2 9	23	1.973	$\bar{3}$ 3 36
21	3.844	$\bar{1}$ 2 12	"	1.970	$\bar{1}$ 3 44
10	3.709	$\bar{1}$ 2 15	9	1.922	$\bar{2}$ 4 24
40	**3.561**	**$\bar{1}$ 2 18**	15	1.908	$\bar{1}$ 3 47
12	3.488	$\bar{2}$ 2 8	6	1.893	$\bar{3}$ 4 20
12	3.440	0 2 10	"	1.889	$\bar{2}$ 4 27
22	3.406	$\bar{1}$ 2 21	9	1.870	$\bar{3}$ 3 42
38	3.302	$\bar{1}$ 1 34	"	1.870	0 3 42
45	3.251	$\bar{1}$ 2 24	9	1.848	$\bar{1}$ 3 50
81	**3.098**	**$\bar{1}$ 2 27**	"	1.847	$\bar{1}$ 4 25
15	3.036	0 2 22	11	1.809	$\bar{2}$ 3 52
13	3.020	0 1 38	"	1.806	$\bar{3}$ 4 29
"	3.014	0 0 42	11	1.802	0 1 68
18	2.951	$\bar{1}$ 2 30	24	1.790	$\bar{1}$ 3 53
100	**2.882**	**$\bar{2}$ 2 26**	"	1.787	0 4 2
90	**2.805**	**0 2 28**	9	1.773	$\bar{2}$ 2 62
28	2.702	$\bar{2}$ 3 1	32	1.752	$\bar{2}$ 3 55
35	2.677	$\bar{1}$ 2 36	"	1.750	$\bar{1}$ 4 34
"	2.673	$\bar{2}$ 3 7	6	1.720	0 4 20
11	2.632	$\bar{1}$ 3 11	10	1.698	$\bar{2}$ 3 58
11	2.578	0 2 34	8	1.671	$\bar{3}$ 3 54
11	2.570	$\bar{1}$ 1 46	"	1.671	0 3 54
7	2.486	$\bar{1}$ 3 20	7	1.651	$\bar{2}$ 2 68
30	2.434	$\bar{1}$ 2 42	9	1.640	$\bar{3}$ 5 1
14	2.426	$\bar{1}$ 3 23	19	1.629	$\bar{1}$ 3 62
70	**2.384**	**$\bar{2}$ 3 25**	12	1.612	$\bar{4}$ 4 34
"	**2.384**	**0 3 0**	3	1.593	$\bar{3}$ 5 19
33	2.365	$\bar{1}$ 3 26	53	1.560	$\bar{1}$ 5 0
18	2.344	0 0 54	19	1.545	0 1 80
56	**2.320**	**$\bar{2}$ 3 28**	"	1.542	$\bar{3}$ 5 28

*Reflection obscured by beamstop, calculated from structure.
The strongest lines are in bold.

TABLE 3. Miscellaneous crystallographic information for wiklundite.

a (Å)	8.257(2)	Crystal size (μm)	3 × 20 × 30
c	126.59(4)	Radiation	Mo$K\alpha$
V (Å^3)	7474(6)	No. of reflections	101,333
Space group	$R\bar{3}c$	No. in Ewald sphere	15497
Z	6	No. unique reflections	1480
D_{calc} (g cm^{-3})	4.072	No. with ($F_o > 4\sigma F$)	1290
		R_{merge} %	6.3
$R_1 = \Sigma(\|F_o\| - \|F_c\|)/\Sigma\|F_c\|$		R_1%	3.2
$wR_2 = [\Sigma w(F_o^2 - F_c^2)^2/\Sigma w(F_o^2)^2]^{1/2}$,		wR_2%	7.6
$w = 1/[\sigma^2(F_o^2) + (0.0335\ P)^2 + 120.99\ P]$			
where $P = (\max(F_o^2,0) + 2F_c^2)/3$			

simulates that of a powder pattern (in much the same way as a Gandolfi camera). The pattern is summarized in Table 2.

Crystal structure: X-ray data collection

A single-crystal fragment (3 μm × 20 μm × 30 μm) of wiklundite was attached to a tapered glass fibre and mounted on a Bruker APEX II ULTRA three-circle diffractometer (at the University of Manitoba, Canada) equipped with a rotating-anode generator (Mo$K\alpha$), multilayer optics and an APEX II 4K CCD detector. A total of 101,333 intensities (15,497 in the Ewald sphere) was collected to $2\theta = 50°$ using 30 s per 0.2° frame with a crystal-to-detector distance of 8 cm. Empirical absorption corrections (*SADABS*; Sheldrick, 2008) were applied, the data were corrected for Lorentz, polarization and background effects, averaged and reduced to structure factors, resulting in 1480 unique reflections. The unit-cell dimensions were obtained by least-squares refinement of the positions of 4059 reflections with $I > 10\sigma I$ and are given in Table 3, together with information pertaining to data collection and structure refinement. The crystal structure of wiklundite was solved by direct methods and refined in the space group $R\bar{3}c$ to an R_1 index of 3.2% (Table 3); atom positions and equivalent isotropic-displacement parameters are given in Table 4, selected interatomic distances in Table 5, refined site-scattering values (Hawthorne *et al.*, 1995) and assigned site populations in Table 6, and bond valences in Table 7. A crystallographic information file has been deposited with the Principal Editor of *Mineralogical Magazine* and is available from http://www.minersoc.org/pages/e_journals/dep_mat.html.

Crystal structure

Cation-site assignment

There are eleven crystallographically distinct cation sites (excluding H) in wiklundite (Table 4). The *Si*(1), *Si*(2) and *Si*(3) sites are tetrahedrally coordinated by O^{2-}. The *Si*(2) and *Si*(3) sites refined to almost exactly 14 eps (electrons per site), and were subsequently fixed as completely occupied by Si in subsequent stages of refinement. The final mean bond lengths of 1.631 and 1.634 Å, respectively, are in accord with their complete occupancy by Si^{4+}. The scattering at the *Si*(1) site refined to ~16.1 eps, and in accord with the formula calculated from the chemical analysis, the occupancy was set as Si_xAs_{1-x} with x considered as variable in subsequent refinement cycles. The *As* site shows triangular pyramidal coordination by O^{2-} with an eps value that indicates complete occupancy by As and a <*As*–O> distance of ~1.79 Å that indicates occupancy by As^{3+}. The *As* site was fixed as completely occupied by As in subsequent stages of refinement. The *M*(1–5) sites are quite diverse in terms of scattering, occupancy and environment. Initial refinement was in accord with almost complete occupancy of all *M* sites by Mn (and Fe). The short <*M*(1)–O> distance of ~2.06 Å indicates occupancy dominantly by Fe^{3+} and the occupancy was so assigned but treated as variable in subsequent stages of refinement. The *M*(2–5) scattering indicates occupancy dominantly by Mn and their occupancies were so assigned but subsequently treated as variable. The refined scattering at the *Pb* site is in accord with occupancy by Pb, and the occupancy was so assigned. The final refined site-scattering values and assigned site-populations are listed in Table 6.

TABLE 4. Atom coordinates and anisotropic-displacement parameters (Å^2) for wiklundite in $R\bar{3}c$.

Atom	Wyckoff symbol	x	y	z	U^{11}	U^{22}	U^{33}	U^{23}	U^{13}	U^{12}	U_{eq}
Pb	12*c*	0	0	0.33772(0)	0.0362(2)	0.0362(2)	0.0233(3)	0	0	0.01811(11)	0.03190(19)
As	12*c*	0	0	0.30601(1)	0.0246(4)	0.0246(4)	0.0203(6)	0	0	0.0123(2)	0.0232(3)
T	18*e*	0	0.73465(18)	¼	0.0287(9)	0.0256(7)	0.0236(10)	–0.0017(3)	–0.0033(6)	0.0144(5)	0.0256(6)
M(1)	12*c*	⅔	⅓	0.28770(1)	0.0236(8)	0.0236(8)	0.0227(11)	0	0	0.0118(4)	0.0233(7)
M(2)	36*f*	0.55471(15)	0.62502(15)	0.26789(1)	0.0243(6)	0.0237(6)	0.0244(7)	0.0003(4)	0.0020(4)	0.0115(5)	0.0244(4)
M(3)	36*f*	0.98277(14)	0.75908(14)	0.28712(1)	0.0240(7)	0.0242(6)	0.0250(7)	–0.0014(4)	–0.0004(4)	0.0126(5)	0.0242(4)
M(4)	36*f*	0.08962(14)	0.44920(14)	0.30581(1)	0.0253(7)	0.0236(6)	0.0247(7)	–0.0012(4)	–0.0011(4)	0.0119(5)	0.0246(4)
M(5)	6*b*	⅔	⅓	⅓	0.0271(11)	0.0271(11)	0.0235(15)	0	0	0.0135(6)	0.0259(9)
Si(1)	12*c*	⅔	⅓	0.25468(2)	0.0234(12)	0.0234(12)	0.0189(17)	0	0	0.0117(6)	0.0219(11)
Si(2)	12*c*	0	0	0.26590(2)	0.0227(10)	0.0227(10)	0.0160(16)	0	0	0.0113(5)	0.0205(7)
Si(3)	12*c*	⅓	⅔	0.28417(2)	0.0210(10)	0.0210(10)	0.0174(16)	0	0	0.0105(5)	0.0198(7)
O(1)	12*c*	⅔	⅓	0.24164(6)	0.029(3)	0.029(3)	0.019(4)	0	0	0.0148(14)	0.0260(18)
O(2)	36*f*	0.8721(6)	0.4931(6)	0.25923(4)	0.024(2)	0.021(2)	0.024(3)	0.0013(19)	–0.002(2)	0.009(2)	0.0239(11)
O(3)	12*c*	0	0	0.27871(6)	0.029(3)	0.029(3)	0.013(4)	0	0	0.0146(14)	0.0238(18)
O(4)	36*f*	0.0596(6)	0.2064(6)	0.26114(4)	0.028(3)	0.021(2)	0.027(3)	0.001(2)	0.002(2)	0.013(2)	0.0247(11)
O(5)	12*c*	⅓	⅔	0.29700(6)	0.027(3)	0.027(3)	0.018(4)	0	0	0.0137(14)	0.0245(18)
O(6)	36*f*	0.1722(6)	0.7028(7)	0.27903(4)	0.022(2)	0.031(3)	0.023(3)	–0.000(2)	0.0005(19)	0.015(2)	0.0245(10)
O(7)	36*f*	0.0272(6)	0.1956(6)	0.29844(4)	0.029(3)	0.020(2)	0.023(3)	0.001(2)	0.000(2)	0.013(2)	0.0233(10)
OH(1)	36*f*	0.1538(7)	0.6884(7)	0.31599(4)	0.026(3)	0.026(3)	0.032(3)	–0.001(2)	0.001(2)	0.013(2)	0.0281(11)
OH(2)	36*f*	0.6123(6)	0.1100(7)	0.29748(4)	0.023(3)	0.027(3)	0.027(3)	0.001(2)	0.001(2)	0.011(2)	0.0265(11)
OH(3)	36*f*	0.8239(6)	0.2626(6)	0.27845(4)	0.026(3)	0.022(2)	0.026(3)	0.002(2)	0.001(2)	0.012(2)	0.0250(11)
Cl	36*f*	0.5834(3)	0.0507(3)	0.34483(2)	0.0318(10)	0.0358(10)	0.0379(11)	0.0079(8)	–0.0001(8)	0.0169(8)	0.0352(5)
H(1)	36*f*	0.035(7)	0.679(13)	0.3182(8)	0.078(19)*						
H(2)	36*f*	0.699(11)	0.163(14)	0.3034(5)	0.078(19)*						
H(3)	36*f*	0.751(12)	0.206(14)	0.2720(5)	0.078(19)*						

*Constrained to be equal during refinement.

TABLE 5. Selected interatomic distances (Å) and angles (°) for wiklundite.

Pb–OH(1)	2.277(5) ×3	*M*(2)–O(1)	2.355(4)
Pb–Cl	3.437(2) ×3	*M*(2)–O(2)	2.164(5)
Pb–Cl	3.776(2) ×3	*M*(2)–O(4)	2.111(5)
<*Pb*–Φ>	3.164	*M*(2)–O(6)	2.273(5)
		M(2)–O(6)	2.329(5)
As–O(7)	1.793(5) ×3	*M*(2)–OH(3)	2.266(5)
		<*M*(2)–Φ>	2.250
Si(1)–O(1)	1.650(8)		
Si(1)–O(2)	1.647(5) ×3	*M*(3)–O(3)	2.197(4)
<*Si*(1)–O>	1.648	*M*(3)–O(6)	2.107(5)
		M(3)–O(7)	2.193(5)
Si(2)–O(3)	1.622(8)	*M*(3)–O(7)	2.337(5)
Si(2)–O(4)	1.634(5) ×3	*M*(3)–OH(2)	2.275(5)
<*Si*(2)–O>	1.631	*M*(3)–OH(3)	2.160(5)
		<*M*(3)–Φ>	2.212
Si(3)–O(5)	1.624(8)		
Si(3)–O(6)	1.637(5) ×3		
<*Si*(3)–O>	1.634		
		M(4)–O(5)	2.215(4)
M(1)–OH(2)	2.075(5) ×3	*M*(4)–O(7)	2.108(5)
M(1)–OH(3)	2.039(5) ×3	*M*(4)–OH(1)	2.189(5)
<*M*(1)–OH>	2.057	*M*(4)–OH(1)	2.190(5)
		M(4)–OH(2)	2.178(5)
		M(4)–Cl	2.682(2)
		<*M*(4)–Φ>	2.260
		M(5)–Cl	2.536(2) ×6
T as tetrahedron		*T* as octahedron	
T–O(2)	2.086(5) ×2	*T*–O(2)	2.086(5) ×2
T–O(4)	2.070(5) ×2	*T*–O(4)	2.070(5) ×2
<*T*–O>	2.078	*T*–O(4)′	2.742(5) ×2
O(4)–*T*–O(4)	116.3(3)	O(4)–*T*–O(4)	96.2(2)
O(2)–*T*–O(4)	102.2(2) ×2	O(2)–*T*–O(4)	86.9(2) ×2
O(2)–*T*–O(4)	122.0(2) ×2	O(2)–*T*–O(2)	90.7(3)
O(2)–*T*–O(2)	90.7(3)	O(4)–*T*–O(4)	74.0(2) ×2
		O(4)–*T*–O(4)	64.5(2) ×2
		O(4)–*T*–O(2)	102.2(2) ×2
		O(4)–*T*–O(2)	122.0(2) ×2

OH(1)–Cl	3.167(5)	H(1)···Cl	2.195(15)	OH(1)–H(1)–Cl	171(9)
OH(2)–Cl	3.579(5)	H(2)···Cl	2.62(2)	OH(2)–H(2)–Cl	167(8)
OH(3)–O(2)	2.847(7)	H(3)···O(2)	1.871(14)	OH(3)–H(3)–O(2)	173(10)

The refined site-scattering of 76.4(6) epfu at the *T* site results from the presence of dominant Mn^{2+} and minor Zn; the assigned site-population of $Mn_{2.70}Zn_{0.30}$ gives 76.5 epfu, and accounts for all Zn measured by electron-microprobe analysis (Tables 1, 6). In kraisslite, the tetrahedrally coordinated *Zn*(1) and *Zn*(2) sites of the $m = 0$ layer (i.e. those sites corresponding to the *T* site in wiklundite) are Zn-dominant and occupied by $^{Zn(1)}(Zn_{0.75}Mn^{2+}_{0.25})$ and $^{Zn(2)}(Zn_{0.72}Mn^{2+}_{0.28})$ with <*Zn*(1)–O> and <*Zn*(2)–O> distances of 1.995 and 1.996 Å, respectively (Cooper and Hawthorne, 2012). In arakiite, a structurally related Zn–Mn^{2+}–Fe^{3+} bearing hydroxylated arsenate-arsenite, the *T*(1) tetrahedron of the $m = 0$ layer is occupied by $(Zn_{0.71}Mn^{2+}_{0.29})$ with a <*T*(1)–O> distance of 1.99 Å, very similar to the *Zn*(1) and *Zn*(2) tetrahedra in kraisslite (Cooper and Hawthorne, 1999). The ionic

TABLE 6. Site-scattering values (epfu) and site populations (apfu) in wiklundite.

	SREF	Pb	As^{3+}	As^{5+}	Si	Zn	Mn^{2+}	Ca	Mg	Fe^{3+}	Al	e^-
Pb	164	2.00										164
As	66		2.00									66
T	76.4(6)					0.30	2.70					76.5
M(1)	50.2(5)						0.20			1.76	0.04	51.3
M(2)	148.7(9)*											
M(3)	150.3(8)*						18.72	0.05	0.23			471.8
M(4)	150.0(8)*											
M(5)	26.2(3)*											
Si(1)	32.2(4)			0.21	1.79							32.0
Si(2)	28				2.00							28
Si(3)	28				2.00							28
Sum	920.0	2.00	2.00	0.21	5.79	0.30	21.62	0.05	0.23	1.76	0.04	917.6

SREF – results from structure refinement. *$\Sigma^{SREF}[M(2)–M(5)] = 475.2$ epfu.

radii of $^{[4]}Zn$ and $^{[4]}Mn^{2+}$ are 0.60 and 0.66 Å, respectively (Shannon, 1976), and the larger <*T*–O> distance of 2.078 Å in wiklundite is in accord with a tetrahedron occupied dominantly by Mn^{2+}. The *T* tetrahedron in wiklundite shows significant deviation in the O–T–O angles from the ideal value of 109.5° (Table 5); a similar distortion is also present in the *Zn*(1) and *Zn*(2) tetrahedra in kraisslite (Cooper and Hawthorne, 2012). In wiklundite, there are two additional anions, O(4), that are 2.742(5) Å from the *T* cation; if considered as bonded to the T cation, the resulting coordination is a very distorted octahedron. This unusual octahedral coordination gives closer to ideal bond-valence sums at both the *T* site and O(4) anion than tetrahedral coordination (Table 7). We have chosen to assign tetrahedral coordination to the *T* site in wiklundite, but also recognize its unusual geometric character.

Anion-site assignment

From its site-scattering and bond lengths to *M*(5) (= Mn^{2+}), the *Cl* site is occupied by Cl. At the final stages of refinement, three additional anions were identified as monovalent *via* their incident bond-valences (Table 7), and these anions are labelled OH(1–3). Their associated H atoms were identified on difference-Fourier maps and their positions and isotropic-displacement parameters were refined with the isotropic-displacement parameters constrained to be equal and the O–H distances constrained to be 0.980(1) Å.

Structure topology

Here, we describe briefly the five distinct polyhedron layers in wiklundite and their stacking. A separate manuscript on the crystal structures of mcgovernite and carlfrancisite is currently underway and will include a discussion of the relation between these structures there. We designate the polyhedron layers as $m = 0$ to 4, as was done for kraisslite (Cooper and Hawthorne, 2012).

The $m = 0$ layer consists of corner-sharing *T* (Mn^{2+} dominant) and *Si*(1) tetrahedra occurring at the vertices of a 12^3 net (Fig. 5*a*). Formally, 3-connected *Si*(1) tetrahedra occur at the vertices of a 6^3 net and *T* tetrahedra are inserted 2-connected vertices (Hawthorne, 2015), an arrangement found in several sheet-silicate minerals. The $m = 1$ layer consists of trimers of edge-sharing *M*(2) octahedra that share vertices with *Si*(2) tetrahedra (Fig. 5*b*). The free peripheral vertices on the upper surface of the trimers are terminated by H(3) atoms that project along the sides of vacant octahedra and hydrogen-bond to the free peripheral vertices [O(2)] on the lower surface of the adjacent trimers (Tables 5, 7), and the apical vertices of the *Si*(2) tetrahedra all point upward in Fig. 5*b*.

The $m = 2$ layer consists of trimers of edge-sharing *M*(3) octahedra that link via *Si*(3) tetrahedra and edge-sharing *M*(1) octahedra (Fe^{3+} dominant) (Fig. 5*c*). Note that in the plane of the sheet, the trimers and the tetrahedra in this layer 'point' in the opposite direction to their analogues in the $m = 1$ layer, indicating that the octahedron-tetrahedron part of each layer is approximately related by

TABLE 7. Bond-valence[1] table for wiklundite.

	Pb	*As*	*T*	*Si*(1)	*Si*(2)	*Si*(3)	*M*(1)	*M*(2)	*M*(3)	*M*(4)	*M*(5)	Σ	H(1)	H(2)	H(3)	Σ
O(1)				0.98				0.22 $^{\times 3}\rightarrow$				1.64				1.64
O(2)			0.45 $^{\times 2}\downarrow$	0.99 $^{\times 3}\downarrow$				0.36				1.80			0.20	2.00
O(3)					1.01				0.33 $^{\times 3}\rightarrow$			2.00				2.00
O(4)			0.47 $^{\times 2}\downarrow$		0.97 $^{\times 3}\downarrow$			0.42				1.94				1.94
			0.08 $^{\times 2}\downarrow$													
O(5)						1.00				0.32 $^{\times 3}\rightarrow$		1.96				1.96
O(6)						0.97 $^{\times 3}\downarrow$		0.27	0.42			1.89				1.89
								0.23								
O(7)		0.99 $^{\times 3}\downarrow$							0.34	0.42		1.98				1.98
									0.23							
OH(1)	0.55 $^{\times 3}\downarrow$									0.34		1.23	0.80			2.03
										0.34						
OH(2)							0.43 $^{\times 3}\downarrow$		0.27	0.35		1.05		0.90		1.95
OH(3)							0.47 $^{\times 3}\downarrow$	0.28	0.37			1.12			0.80	1.92
Cl	0.09 $^{\times 3}\downarrow$									0.22	0.33 $^{\times 6}\downarrow$	0.67	0.20	0.10		0.97
	0.03 $^{\times 3}\downarrow$															
Σ	2.01	2.97	2.00	3.95	3.92	3.91	2.70	1.78	1.96	1.99	1.98		1.00	1.00	1.00	

[1]Calculated with the parameters of Brown (1981) and Brese and O'Keeffe (1991).

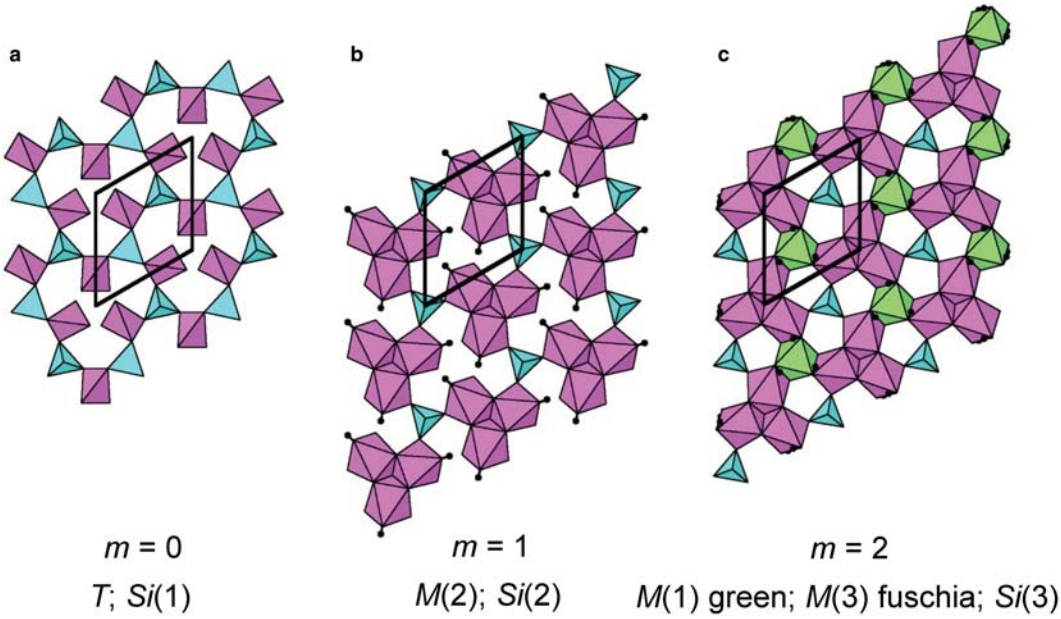

FIG. 5. The $m = 0,1,2$ polyhedron layers in wiklundite. Mn^{2+} dominant = fuschia, Fe^{3+} dominant = green, Si dominant = blue. H atoms = black circles. Unit cell outline in black.

rotation of 180° about an axis || **c**. The *M*(1) octahedron occupies a position corresponding to the vacant octahedron in the $m = 1$ layer and the constituent anions are entirely (OH) groups (Table 5). The $m = 3$ layer (Fig. 6*a*) consists of trimers of edge-sharing *M*(4) octahedra linked by AsO_3 triangular pyramids, and the orientation of the layer is the same as that of the $m = 1$ layer (Fig. 5*b*). The linking vertices [O(7)] occur on the lower level of the layer (Fig. 6*a*), and the remaining anions of the lower level are (OH) groups [OH(2)] at the periphery of a trimer and O^{2-} [O(5)] at the

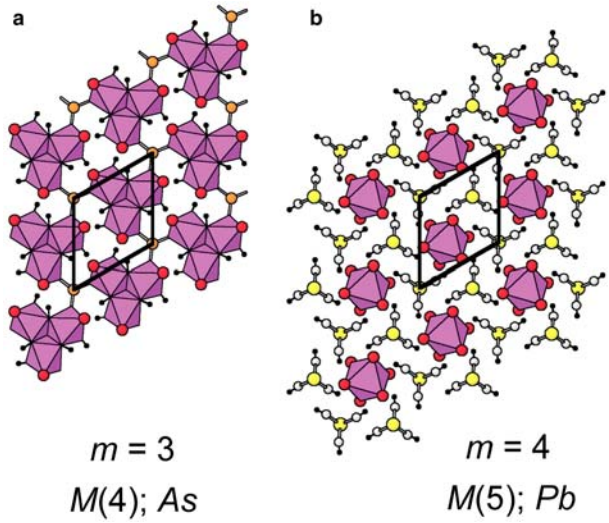

FIG. 6. The $m = 3,4$ polyhedron layers in wiklundite. Legend as in Fig. 5, with As^{3+} atoms = orange circles, Pb atoms = yellow circles, Cl atoms = red circles, (OH) groups = grey circles.

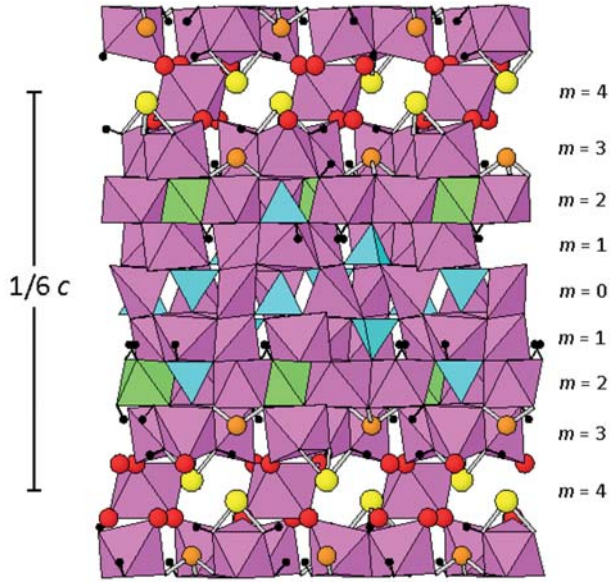

FIG. 7. Stacking of polyhedron layers ($m = 0$ through $m = 4$) in wiklundite. Legend as in Figs 5 and 6.

centre of the trimer. All anions of the upper level of the sheet are monovalent; the anions shared between *M*(4) octahedra are (OH) groups [OH(1)] whereas the anions that belong to only one *M*(4) octahedron are Cl. (Fig. 6*a*). The H(1) and H(2) atoms hydrogen-bond to the Cl atom (Tables 5, 7). The $m = 4$ layer consists of isolated $M(5)Cl_6$ octahedra, each surrounded by six $Pb(OH)_3$ pyramids (Fig. 6*b*), with additional weak Pb–Cl and H···Cl linkages (Tables 5, 7).

The stacking sequence of polyhedron layers in wiklundite is shown along 1/6 **c** (Fig. 7). Two sets of $m = 0$–4 layers occur in this section of the structure, and there is a reversal of stacking sequence across the $m = 0$ layer. The $m = 4$ layer is particularly prominent in this view. Because of the large radii of the Cl^- and Pb^{2+} ions, the $m = 4$ layer is much thicker than the other layers, but the apparent 'holes' in the layer are illusory: the space is occupied by the stereoactive lone-pairs of electrons of Pb^{2+}, long Pb–Cl bonds, and H···Cl hydrogen bonds.

Low bond valence at O(1)

Inspection of Table 7 shows that the sum of the bond valences incident at O(1) is 1.64 valence units (vu). The [4]-coordinated O(1) anion links the *Si*(1) tetrahedron in the $m = 0$ layer to the centre of the trimer of *M*(2) octahedra in the $m = 1$ layer, and does not receive any bond valence from hydrogen bonds (Tables 5, 7, Figs 5*a*,*b*). The bond-valence sum at the *M*(2) site is also somewhat low at 1.78 vu. The <*M*(2)–O> distance of 2.25 Å is reasonable for a $^{[6]}Mn^{2+}$-dominant site, and for comparison, the Mn^{2+}-dominant *M*(4) site with a comparable <*M*(4)–O> distance of 2.26 Å has a near-ideal bond-valence sum of 1.99 vu. In kraisslite a very similar bond-valence anomaly is present (Cooper and Hawthorne, 2012). In kraisslite, the topologically identical $m = 0$ and $m = 1$ layers connect in the same manner as in wiklundite, via the O(8) anion (i.e. the analogue of O(1) in wiklundite) which is shared between the Si-dominant *T*(2) tetrahedron of the $m = 0$ layer and the Mn^{2+}-dominant *M*(2)–*M*(3)–*M*(12) trimer of the $m = 1$ layer. This O(8) anion has a noticeable low bond-valence sum of 1.73 vu, and the *M*(2), *M*(3) and *M*(12) bond-valence sums are also somewhat low at 1.83, 1.84 and 1.84 vu, respectively. We therefore regard the low bond-valence sums at O(1) and *M*(2) in wiklundite and at O(8) and *M*(2), *M*(3) and *M*(12) in kraisslite as features of the two (similar) structures that are indicative of structural strain associated with connectivity of the $m = 0$ and $m = 1$ layers in both minerals.

Heterovalent substitution

The *M*(1) site is occupied dominantly by Fe^{3+}, and also contains 10% divalent cations (Mn^{2+}).

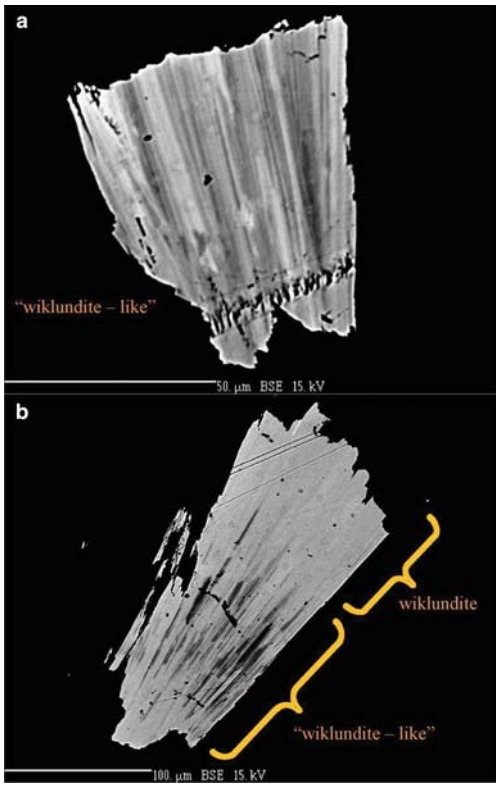

FIG. 8. Back-scattered-electron image of wiklundite and 'wiklundite-like' material; (*a*) a section of a sheaf-like aggregate of 'wiklundite-like' material near its mid-section; (*b*) a sheaf-like aggregate, with the outer region of the aggregate intact at the upper-right of the image.

The *Si*(1) site is occupied dominantly by Si, and also contains 10% pentavalent cations (As^{5+}) (Table 6). The *M*(1) and *Si*(1) sites have the same multiplicity, and a net offsetting heterovalent exchange (pfu) can be written as:

$$^{M(1)}Fe^{3+}_{0.2} + {}^{Si(1)}Si^{4+}_{0.2} \leftrightarrow {}^{M(1)}Mn^{2+}_{0.2} + {}^{Si(1)}As^{5+}_{0.2}$$

The *Si*(1) tetrahedron occurs in the $m = 0$ layer and the *M*(1) octahedron in the $m = 2$ layer (Figs 5*a*,*c*), and therefore the heterovalent substitutions do not couple directly through common anions. In comparison, the *M*(13) octahedron in kraisslite contains 50% divalent ($Mn^{2+} > Mg$) and 50% trivalent ($Fe^{3+} > Al$) cations, with a concomitant substitution of minor As^{5+} over several Si-dominant tetrahedra.

Wiklundite and 'wiklundite-like' material

Many attempts were made to retrieve single crystals suitable for single-crystal structure refinement, but only two high-quality crystals could be recovered. Most crystals show significant diffraction complexity with regard to indexing reflections along the **c** axis. The two high-quality wiklundite single-crystals were extracted from the outer margin of two different sheaf-like aggregates, and give near-identical structure-refinement results. Both structures are well-ordered with fully occupied $Pb(OH)_3$–$MnCl_6$ layers. As these high-quality single-crystals are extremely rare and very thin (~3 µm), we did not want to risk losing them by preparing them for electron-microprobe analysis. Several other larger grains were prepared for EMPA, and one such fragment is shown in back-scattered-electron-imaging mode (Fig. 8*a*). This grain is ~50 µm across and is composed of finely alternating and interpenetrating subparallel elongated zones of variable image brightness. A 5 µm electron beam was used to analyse regions of different grey-level brightness, and corresponding values of 6.1 to 10.5 wt.% PbO were measured. As the beam diameter exceeds the widths of the individual compositional zones, each analytical point is an average of several zones. This particular fragment is a section of a sheaf-like aggregate near its midsection. Figure 8*b* is a back-scattered-electron image of another sheaf-like aggregate, with the outer terminal region of the aggregate intact at the upper-right part of the image. Ten EMPA points acquired from the outer ~1/3 of this aggregate near its terminus gave high and uniform values of PbO: 14.6–15.3 wt.%, in agreement with the Pb content from the refined wiklundite structure. Two additional point analyses centred on darker grey-level regions further down the aggregate gave values of 9.6 and 10.2 wt.% PbO. The $Pb(OH)_3$–$MnCl_6$ layer in wiklundite has a rather specific stereochemistry: lone-pair stereoactive $Pb(OH)_3$ pyramids in combination with Mn^{2+} cations octahedrally coordinated by large Cl atoms. Chemical variation in such a distinctive layer is not anticipated, other than $Mn^{2+} \leftrightarrow$ (Mg, Fe^{2+}) substitution. In Fig. 9, the variation in PbO is shown as a function of Cl for the electron-microprobe analyses acquired from the grains in Fig. 8. The circled cluster of points conforming to wiklundite has a wt.% Cl/wt.% PbO value of ~0.43. A (hand-drawn) line through the remaining data points conforms to this ratio, suggesting that for the lower Pb content (i.e. 6.1–10.5 wt.% PbO), a fully occupied $Pb(OH)_3$–$MnCl_6$

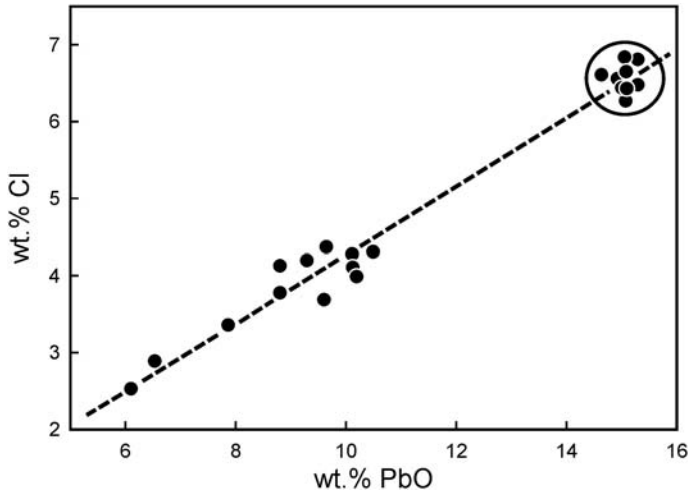

FIG. 9. Variation in Cl content as a function of PbO content in wiklundite (high PbO) and 'wiklundite-like' material (low PbO).

layer is present but occurs with less frequency in the stacking sequence relative to its frequency in the wiklundite stacking sequence. We refer to this lower-Pb material as a 'wiklundite-like' mineral. Many attempts were made to retrieve a suitable crystal of low-Pb composition for structure solution and refinement. However, all crystals gave complex diffraction patterns that could not be properly indexed along the **c** axis. The variable and overlapping diffraction along the **c** axis results from several superimposed diffraction patterns from domains with different repeats along **c***. Each domain contains a different insertion frequency of the $Pb(OH)_3$–$MnCl_6$ layer, and hence a different PbO and Cl content with a constant Cl:PbO ratio. Physical sampling of a uniform chemistry and structure for a 'wiklundite-like' region is not possible due to the very fine scale of the variation. The majority of a given radiating sheaf-like aggregate contains the low-Pb wiklundite-like material, with wiklundite occurring along the outer margin.

Acknowledgements

We thank Thomas Armbruster and Peter Leverett for their comments on the paper. Financial support for this work came from the Natural Sciences and Engineering Research Council of Canada in the form of a Canada Research Chair in Crystallography and Mineralogy, and a Discovery grant to FCH, and by Canada Foundation for Innovation grants to FCH.

References

Araki, T. and Moore, P.B. (1981) Dixenite, $Cu^{1+}Mn^{2+}_{14}Fe^{3+}(OH)_6(As^{3+}O_3)_5(Si^{4+}O_4)_5(As^{5+}O_4)$: metallic $[As^{3+}_4Cu^{1+}]$ clusters in an oxide matrix. *American Mineralogist*, **66**, 1263–1273.

Boström, K., Rydell, H. and Joensuu, O. (1979) Långban – An exhalative sedimentary deposit? *Economic Geology*, **74**, 1002–1011.

Brese, N.E. and O'Keeffe, M. (1991) Bond-valence parameters for solids. *Acta Crystallographica*, **B47**, 192–197.

Brown, I.D. (1981) The bond-valence method: an empirical approach to chemical structure and bonding. Pp. 1–30 in: *Structure and Bonding in Crystals II* (M. O'Keeffe and A. Navrotsky, editors). Academic Press, New York.

Brugger, J., Armbruster, T., Meisser, N, Hejny, C. and Grobety, B. (2001) Description and crystal structure of turtmannite, a new mineral with a 68 Å period related to mcgovernite. *American Mineralogist*, **86**, 1494–1505.

Christy, A.G. and Gatedal, K. (2005) Extremely Pb-rich rock-forming silicates including a beryllian scapolite and associated minerals in a skarn from Långban, Värmland, Sweden. *Mineralogical Magazine*, **69**, 995–1018.

Coey, J.M.D. (1984) Mössbauer spectroscopy of silicate minerals. Pp. 443–509 in: *Mössbauer Spectroscopy Applied to Inorganic Chemistry* (G.J. Long, editor). Plenum Press, New York and London.

Cooper, M.A. and Hawthorne, F.C. (1999) The effect of differences in coordination on ordering of polyvalent cations in close-packed structures: the crystal structure

of arakiite and comparison with hematolite. *The Canadian Mineralogist*, **37**, 1471–1482.

Cooper, M.A. and Hawthorne, F.C. (2001) The biggest mineral: The crystal structure of mcgovernite. *Eleventh Annual V.M.Goldschmidt Conference*, abstract #3446.

Cooper, M.A. and Hawthorne, F.C. (2012) The crystal structure of kraisslite, $^{[4]}Zn_3(Mn,Mg)_{25}(Fe^{3+},Al)(As^{3+}O_3)_2[(Si,As^{5+})O_4]_{10}(OH)_{16}$, from the Sterling Hill mine, Ogdensburg, Sussex County, New Jersey, USA. *Mineralogical Magazine*, **76**, 2819–2836.

Flink, G. (1920) Trigonite and dixenite, two new minerals from the Långbanshytte mines. *Geologiska föreningens i Stockholm förhandlingar*, **42**, 436–452 [in Swedish].

Grew, E.S., Yates, M.G., Belakovskiy, D.I., Rouse, R.C., Su, S.C. and Marquez, N. (1994) Hyalotekite from reedmergnerite-bearing peralkaline pegmatite, Dara-i-Pioz, Tajikistan and from Mn skarn, Långban, Värmland, Sweden: A new look at an old mineral. *Mineralogical Magazine*, **58**, 285–297.

Hawthorne, F.C. (2015) Generating functions for stoichiometry and structure of single- and double-layer sheet-silicates. *Mineralogical Magazine*, **79**, 1675–1709.

Hawthorne, F.C. and Della Ventura, G. (2007) Short-range order in amphiboles. Pp. 173–222 in: *Amphiboles: Crystal Chemistry, Occurrence and Health Issues* (F.C. Hawthorne, R. Oberti, G. Della Ventura and A. Mottana, editors.) Reviews in Mineralogy and Geochemistry, **67**. Mineralogical Society of America and Geochemical Society, Washington D.C.

Hawthorne, F.C, Ungaretti, L. and Oberti, R. (1995) Site populations in minerals: terminology and presentation of results of crystal-structure refinement. *The Canadian Mineralogist*, **33**, 907–911.

Hawthorne, F.C., Abdu, Y.A., Ball, N.A. and Pinch, W.W. (2013) Carlfrancisite: $Mn_3^{2+}(Mn^{2+},Mg,Fe^{3+},Al)_{42}[As^{3+}O_3]_2(As^{5+}O_4)_4[(Si,As^{5+})O_4]_6[(As^{5+},Si)O_4]_2(OH)_{42}$, a new arseno-silicate mineral from the Kombat mine, Otavi Valley, Namibia. *American Mineralogist*, **98**, 1693–1696.

Holtstam, D. and Langhof, J. (1999) *Långban. The Mines, their Minerals, Geology and Explorers*. Swedish Museum of Natural History & Raster Förlag, Stockholm, 215 pp.

Holtstam, D. and Mansfeld, J. (2001) Origin of a carbonate-hosted Fe-Mn-(Ba-As-Pb-Sb-W) deposit of Långban-type in Central Sweden. *Mineralium Deposita*, **36**, 641–657.

Jernberg, P. and Sundqvist, T. (1983) *A Versatile Mössbauer Analysis Program*. Uppsala University, Institute of Physics, UUIP-1090.

Magnusson, N.H. (1930) The Långban ore district. *Sveriges Geologiska Undersökning, Serie Ca*, **23**, 1–111. [in Swedish].

Moore, P.B. and Ito, J. (1978) Kraisslite, a new platy arsenosilicate from Sterling Hill, New Jersey. *American Mineralogist*, **63**, 938–940.

Palache, C. and Bauer, L.H. (1927) Mcgovernite, a new mineral from Sterling Hill, New Jersey. *American Mineralogist*, **12**, 373–374.

Pouchou, J.L. and Pichoir, F. (1985) '*PAP*' $\varphi(\rho Z)$ procedure for improved quantitative microanalysis. Pp. 104–106 in: *Microbeam Analysis* (J.T. Armstrong, editor). San Francisco Press, San Francisco, California, USA.

Roberts A.C., Grice J.D., Cooper M.A., Hawthorne F.C. and Feinglos M.N. (2000) Arakiite, a new Zn-bearing hematolite-like mineral from Långban, Värmland, Sweden. *The Mineralogical Record*, **31**, 253–256.

Shannon, R.D. (1976) Revised effective ionic radii and systematic studies of interatomic distances in halides and chalcogenides. *Acta Crystallographica*, **A32**, 751–767.

Sheldrick, G.M. (2008) A short history of SHELX. *Acta Crystallographica*, **A64**, 112–122.

Wuensch, B.J. (1960) The crystallography of mcgovernite, a complex arsenosilicate. *American Mineralogist*, **45**, 937–945.